


Formation of parallel and perpendicular ripples on solid amorphous surfaces by ion beam-driven atomic flow on and under the surface

Alvaro Lopez-Cazalilla *, Kai Nordlund, and Flyura Djurabekova

Helsinki Institute of Physics and Department of Physics, University of Helsinki, P.O. Box 43, Helsinki FI-00014, Finland



(Received 23 November 2022; revised 4 February 2023; accepted 16 March 2023; published 30 March 2023)

The off-normal ion irradiation of semiconductor materials is seen to induce nanopatterning effects. Different theories are proposed to explain the mechanisms that drive self-reorganization of amorphizable surfaces. One of the prominent hypothesis associates formation of nanopatterning with the changes of sputtering characteristics caused by changes in surface morphology. At ultralow energy, when sputtering is negligible, the Si surface has still been seen to reorganize forming surface ripples with the wave vector is either aligned with the ion beam direction or perpendicular to it. In this work, we investigate the formation of ripples using molecular dynamics in all the three regimes of ripple formation: low angles where no ripples form, intermediate regime where the ripple wave vectors are parallel to the beam, and high angles where they are perpendicular to it. We obtain atom-level insight on how the ion-beam driven atomic dynamics at the surface contributes to organization, or lack of it, in all the different regimes. Results of our simulations agree well with experimental observations in the same range of ultralow energy of ion irradiation.

DOI: [10.1103/PhysRevMaterials.7.036002](https://doi.org/10.1103/PhysRevMaterials.7.036002)

I. INTRODUCTION

Surface self-organization is an interesting phenomenon and seen at different scales in time and in space, if the surface is exposed to momentum transfer at tilted incidence. For instance, the blowing wind or the running water can develop ripples on sand surfaces the ripples aligned either parallel or perpendicular to the wind direction [1]. The mechanisms behind this was explained by Bagnold [2], observing that the grains move according to the *reptation* and *saltation* processes.

Under ion beam irradiation of semiconductor materials, the momentum is transferred to the surface via individual ion impacts. Collectively, these impacts may induce patterning on the surface of the material similar to the sand ripples and dunes. The ion-beam-induced nanopatterning effect was observed the first time in the 1960s by Cunningham [3] in Au using 8 keV-Ar⁺ at 70° off-normal incidence. Since then, many theories have been developed in order to explain the ripple formation with the focus on erosion [4], atom redistribution [5,6], and stress build-up [7–10]. The structures observed in experiments range from ordered nanodots in GaSb [11] and in Si [12] (with sample rotation) to parallel [13] and perpendicular to the ion-beam projection ripples (i.e., the wave vector direction) [14].

Computational methods like molecular dynamics (MD) or the binary collision approximation (BCA) have been used extensively to study this curious phenomenon. The application of these methods has shed light on some of the aspects of it. Norris *et al.* [15] introduced the crater function formalism which allowed the prediction of the pattern formation and corresponding wavelength of these periodic structures

[6,14,16]. This model was particularly successful if it was based on single-impact MD simulations, emphasizing the importance of small atomic displacements which result from low-energy multibody interactions accessible in MD, but not in BCA [16].

Although single impact simulations have already provided important insights in understanding the mechanisms of nanopattern formation, the main advantage of the MD method is a possibility to simulate cumulative radiation effects due to high fluence irradiation. Under the time and length scale limitation of this type of atomistic modeling, it is, nevertheless, possible to simulate sequential ion impacts to understand the relative contribution of erosion and atomic redistribution on surface modification during prolonged ion irradiation with different energies and at different incident angles [14]. At the same time, we measure the relative effect of structural order of irradiated material with respect to efficiency of surface modification [17]. The results show that the contribution of the erosion contrary to redistribution, is strongly dependent on the material and the ion energy. Recently it was shown that very high fluences in MD simulations can be achieved by using a speed-up algorithm [18]. Applying this algorithm we were able to observe directly the pattern formation in parallel mode on a-Si surface under very low incident energies of 30 eV [19] similar to the ripples observed experimentally [14]. The effect of mass redistribution was confirmed also in other MD simulations [20], where the incident angles between 40° and 70° were studied. However, to our knowledge none of the previous MD simulations were able to elucidate the mechanisms of parallel-to-perpendicular mode transition with increase of incident energy up to the grazing incidence.

In this work, we examine systematically ripple formation over all incident angles to understand why there are no ripples at low incidence angles, and why the ripples turn direction at the highest angles. To understand the formation mechanisms

*alvaro.lopezcazalilla@helsinki.fi

comprehensively, we analyze the atom redistributions separating displacements in the three different dimensions, and in particular examine in detail displacements at very small grazing angles (the incident angle $> 80^\circ$), where the ripples in the perpendicular mode are expected to appear [21]. Moreover, to enable a quantitative analysis of whether self-organization has occurred, we also perform fast Fourier transform (FFT) of the surfaces.

Different quantitative analyses of the simulated data along with the direct observation of the evolution of the irradiated surfaces complement the model presented in Ref. [19] and allow us to complete the picture of ripple formation on amorphous surfaces within a certain range of incident angles at least, at very low near the displacement threshold energies.

II. METHODS

A flat-surface cell of amorphous Si containing 73584 atoms was relaxed [14,17] to 300 K in order to perform the sequential bombardment. The final size of the cell is $16.56 \times 16.56 \times 5.15 \text{ nm}^3$.

The simulations were performed using the PARCAS MD code [22,23]. The Si-Si interactions are described using the environment-dependent inter-atomic potential [24,25], complemented at short distances by the purely repulsive Ziegler-Biersack-Littmark potential [26]. The same type of repulsive potential describes the Ar-Si interaction. The bombardment of the sample is done sequentially [14,17], so we used the pair potential with high energy repulsive part from density functional theory DMol calculations [26] smoothly joined to the Lennard-Jones equilibrium part [27] at larger distances to describe the Ar-Ar interactions.

The irradiation of the sample is done using the speed-up scheme [18], which allows for reaching high fluences using MD simulations [19]. In this study, we used four angles of ion incidence, $\theta = \{0^\circ, 45^\circ, 70^\circ, 85^\circ\}$. The normal incidence is used as a reference case to show how the surface behaves during ion irradiation up to high fluences when the ion beam is not tilted. $\theta = 45^\circ$ provides sufficiently strong tilt, while yet being less than the threshold $\theta = 55^\circ$ [28]. $\theta = 70^\circ$ corresponds to the regime where parallel mode ripples are expected to form (the MD results at this angle were the same as those in Ref. [19], however, in this work we performed additional displacement and Fourier transform analysis on the MD results). $\theta = 85^\circ$ corresponds to the very small grazing incidents, at which the ion is still able to hit the surface. At this angle, the perpendicular mode of ripples was observed in experiments [14] shown in Fig. 1(i).

The 30 eV-Ar⁺ atom is placed above the surface at such a location that when it hits the surface the impact is always at the center independently of the incident angle. The center of the surface is selected for the impact to initiate the cascade far from the border to avoid the interactions over periodic boundaries. For consistency with the tilt of the beam, the azimuthal angle is always fixed and is aligned with the x axis. Despite the fixed entry point, the ion actually impacts always at a random place of the cell because of shifting the cell in both x and y directions prior to every impact.

We simulated 54 000 consecutive ion impacts at the 0° , 45° and 70° reaching the fluence $2 \times 10^{16} \text{ ions cm}^{-2}$, which was

sufficient to observe the high-fluence effects. In the case of 85° , the grazing angle is too small and much higher fluence was needed to observe self-organization of irradiated surface. In this case, we simulated 160 000 consecutive Ar impacts (fluence of $5.9 \times 10^{16} \text{ ions cm}^{-2}$). This is not surprising; in experiments, self-organization of the irradiated surface with grazing angle was also observed at much higher fluences than those for the incident angles closer to the normal [14].

After every nine impacts, the temperature of the system is restored to 300 K applying the Berendsen thermostat [29] during additional 30 ps. Each individual impact is allowed to develop for 1 ps only with the thermostat controlling temperature to 300 K applied to the 0.8 nm-thick layers at the borders of the cell in the x and y directions, but not at the surface. More details on the speedup scheme can be found in Ref. [19].

The erosion and atomic redistribution components of the ripple formation mechanism are computed by counting the number of sputtered atoms in the system, and the total displacement. The total displacement was calculated summing up separately each component of the individual displacement vectors of all atoms displaced in a cascade:

$$\delta_w^q = \sum_{i=1}^{N_{\text{displaced}}} (w_{\text{final}}^i - w_{\text{initial}}^i), \quad (1)$$

where $N_{\text{displaced}}$ is the number of atoms displaced within the cell, the indices *final* and *initial* refer to the current and initial positions of the atoms, respectively, while $w = \{x, y, z\}$. The superscript q is not applied for the w components of the total displacements of atoms in the system, while $q = "+"$ or $"-"$ is used to indicate the positive or negative components of the δ_w , which include separately the atomic displacement along each w axis only in the positive or only in the negative direction, respectively. Moreover, under high fluence ion irradiation the accumulation of stresses is expected due to numerous atomic displacements in multiple cascades. This quantity is also accessible in MD as we showed in Ref. [19]. We attempted to analyze the stress in the current simulations as well, but could not observe any clear relation between the ripple formation and the stress build-up at this low energy.

Fast Fourier transform

To obtain a diffraction-like image of the surfaces (similar to those obtained from the atomic force microscopy (AFM) experiments, the FFT is calculated using the MATLAB toolbox [30]. We considered the last frame simulated at different irradiation angles, where the surface features are the most prominent, enhancing the probability of obtaining a more pronounced result. However, the ridge-trough distance in some of the cases is not marked, so we needed to magnify this difference. In order to do that, we consider 100×100 bins in the $x - y$ plane, containing a small amount of atoms per bin. Among those atoms, we consider the highest atom (z coordinate) in the bin to amplify the differences between the bins that are separated from each other, and consequently, detect more efficiently the possible pattern. Then, the color scale is chosen independently for all the cases, in order to highlight the orientation of any formation.

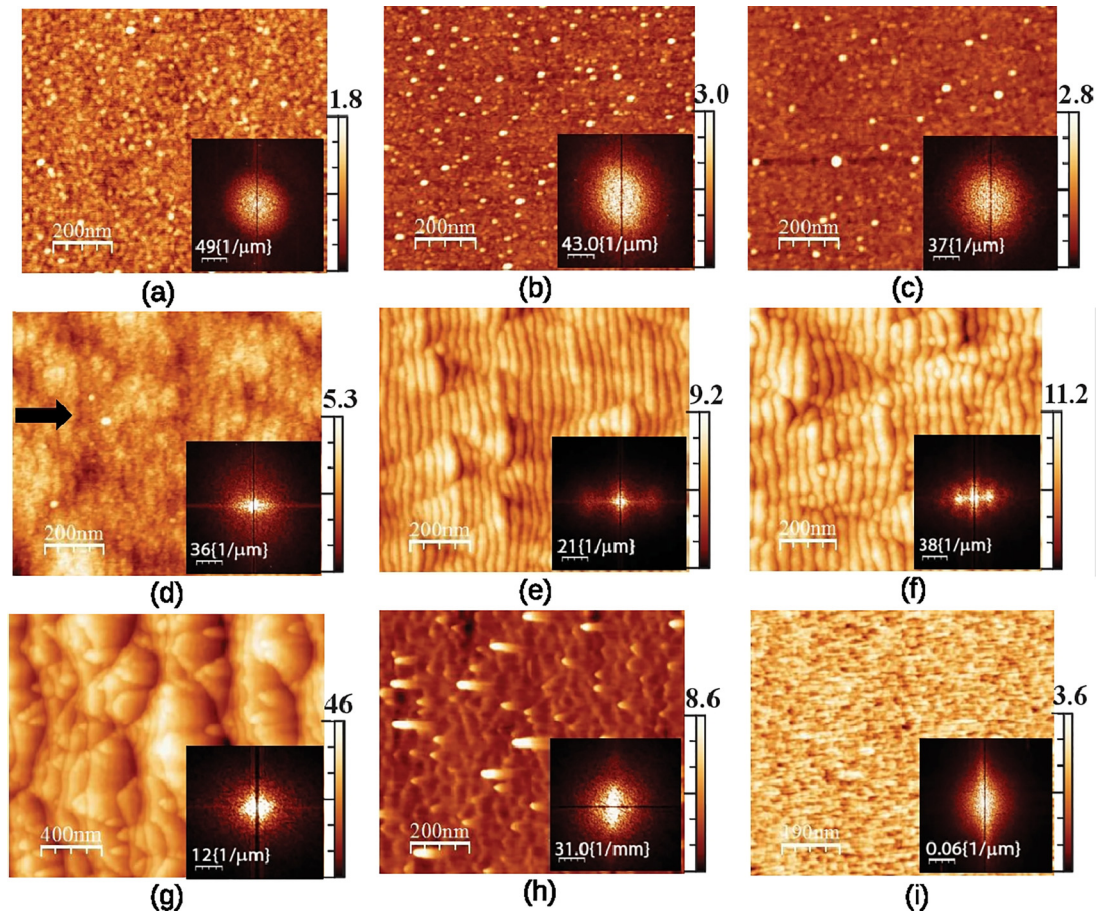


FIG. 1. AFM images of the evolution of morphology at different ion incidence angles: (a) 0° , (b) 25° , (c) 35° , (d) 55° , (e) 65° , (f) 70° , (g) 75° , (h) 80° , and (i) 85° for 30 eV-Ar^+ ion irradiation, current density $52\ \mu\text{A cm}^{-2}$ and fluence $1 \times 10^{19}\text{ ions cm}^{-2}$. The different insets show the corresponding FFT images and the black arrow indicates the beam direction for oblique incidence ion irradiation. The ripples in images (e) and (f) are called parallel mode ripples because the wave vector (see insets) is parallel to the ion beam. The ripples in image (i) are correspondingly called perpendicular mode ripples. Reprint from Ref. [14].

III. RESULTS

A. Surface self-organization

In Figs. 2 and 3 we show the gradual evolution of a-Si surface under ion irradiation with different incidence. Figures 2, 3(a), and 3(b) show the simulation snapshots after 4500 and 54 000 ion impacts on the left and the right sides of the corresponding figures, respectively. Figures 3(c) and 3(d) show similar snapshots but after 78 000 and 160 200 ion impacts, respectively. In the top corner of Figs. 2(b), 2(d), 3(b), and 3(d), we also show the FFT images generated from the analysis of the atoms in the corresponding surfaces for better comparison with the experimental results shown in Fig. 1.

First of all, we observe that under the normal incidence the surface roughness develops rapidly already at the early stage of the irradiation [see Fig. 2(a)]. With fluence increase, the roughness increases as well, forming randomly located mounds, similarly to those observed initially under the 70° incidence in the previous simulations [19]. However, under the normal incidence the mounds do not self-organize, but remain random even at fluence more than an order of magnitude higher, see Fig. 2(b). This behavior persists until the end of the simulation. The absence of a clear surface pattern in this

case is consistent with the AFM measurements in Fig. 1(a). See Supplemental Material 0DEGREES-SURF-FORMATION-DISP.MP4 and 0DEGREES-SURF-FORMATION-POSZ.MP4 [31] for the surface evolution under normal incidence. The random nature of roughness is also confirmed by the FFT image shown in the inset of Fig. 2(b) with no preferential structure, which agrees well with the experimental FFT image in Fig. 1(a).

After tilting the ion beam to 45° off-normal, we also observe significant development of surface roughness at the early stages of irradiation [see Fig. 2(c)]. At a later stage [Fig. 2(d)], the random mounds start organizing in some surface features, however, the process does not complete in any recognizable pattern even at the fluence of $\sim 2 \times 10^{16}\text{ cm}^{-2}$ (for comparison, the clear ripples were formed at the fluence $1.8 \times 10^{16}\text{ cm}^{-2}$ under the 70° incidence as reported in Ref. [19]). Local self-organized ridges seen in Fig. 2(d) do not align in any preferential direction, i.e., neither as parallel- nor perpendicular-mode ripples. See Supplemental Material, 45DEGREES-SURF-FORMATION-DISP.MP4 and 45DEGREES-SURF-FORMATION-POSZ.MP4 for the evolution of surface at 45° incidence [31]. In the FFT image in the inset of Fig. 2(d) we notice that some alignment is emerging. However, this alignment is rather vague, which is explained by the

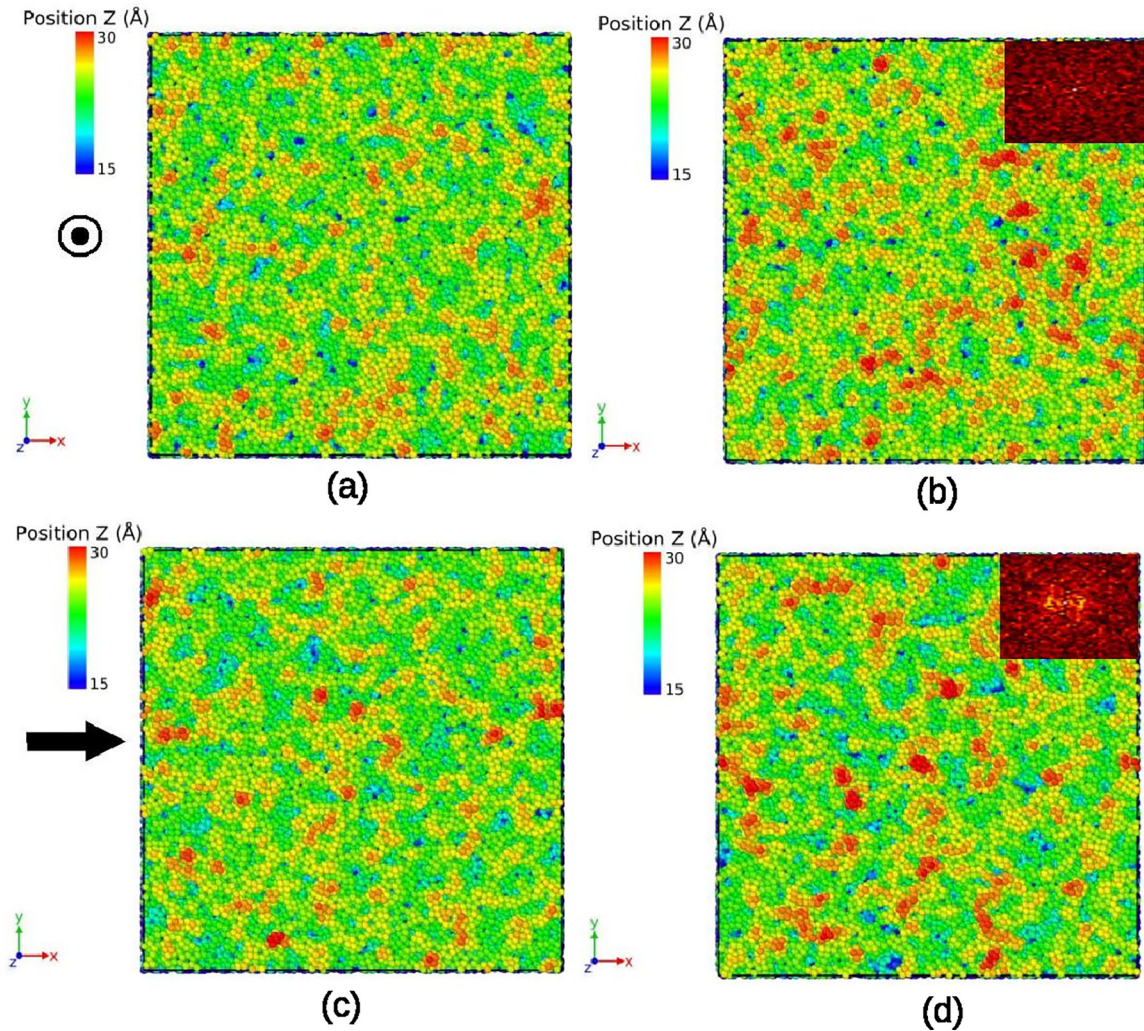


FIG. 2. Evolution of the a-Si surface under 30eV-Ar⁺ at 0° (a) 4500 and (b) 54000 impacts (including FFT of the surface); and at 45° (c) 4500 and (d) 54000 impacts (including FFT of the surface). The black arrow indicates the irradiation direction.

absence of clear periodicity. On the larger experimental surface, this vague pattern is expected to disappear due to higher randomness of orientations of local self-organized features. Unfortunately, there is no experimental data at this angle in Fig. 1, although interpolation between the result shown in Figs. 1(c) and 1(d) is consistent with the above argument.

In Figs. 3(a) and 3(b) we show how the ripples in parallel mode emerge from the initially random surface roughness at 70° incidence. Here we also generated the FFT image for the ripples in Fig. 3(b) that show a clear pattern similar to that obtained for the experimentally observed ripples, see inset of Fig. 1(f). Increasing the incidence angle further to 85° off-normal slows down the dynamics of self-organization. In these simulations, we had to increase the fluence to much higher value to start observing any organizational pattern. Note the difference in the total numbers of ion impacts simulated for this case: Figure 3(c) shows the snapshot for the simulation cell after 78 000 ion impacts (4500 ions for lower incident angles) and Fig. 3(d) after 160 200 ion impacts (54 000 ions for lower incident angles). The necessity of the fluence increase is consistent with the experiments reported in Ref. [14] and is explained by much lower momentum

transfer from ion beam to surface atoms, since many impacts result in backscattering of incident ions. These presented snapshots showing the surface evolution under 85° off-normal incidence, demonstrate the gradual self-organization of the surface into ripples in the perpendicular mode, although the roughening of the surface under the grazing incidence is much slower and shallower [see Fig. 1(i)]. We observe formation of the first mounds at the beginning of the simulation (see 85DEGREES-SURF-FORMATION-POSZ.MP4). As the fluence increases [Fig. 3(c)], these mounds merge with others and some thin ripplelike structures start developing. See Supplemental Material (85DEGREES-SURF-FORMATION-DISP.MP4 and 85DEGREES-SURF-FORMATION-POSZ.MP4) for the complete dynamics [31] This surface reorganization becomes fully clear at the last stages of the simulation [Fig. 3(d)], where the ridges of the ripples align along the projected ion beam forming ripples in the perpendicular mode, i.e., with the wave vector perpendicular to ion beam projection. This result is fully consistent with the experiment from Ref. [14] where the rotation of the ripples was also observed at 85°, but the wavelength of these periodic structures could not be measured due to the low roughness for this irradiation angle. In

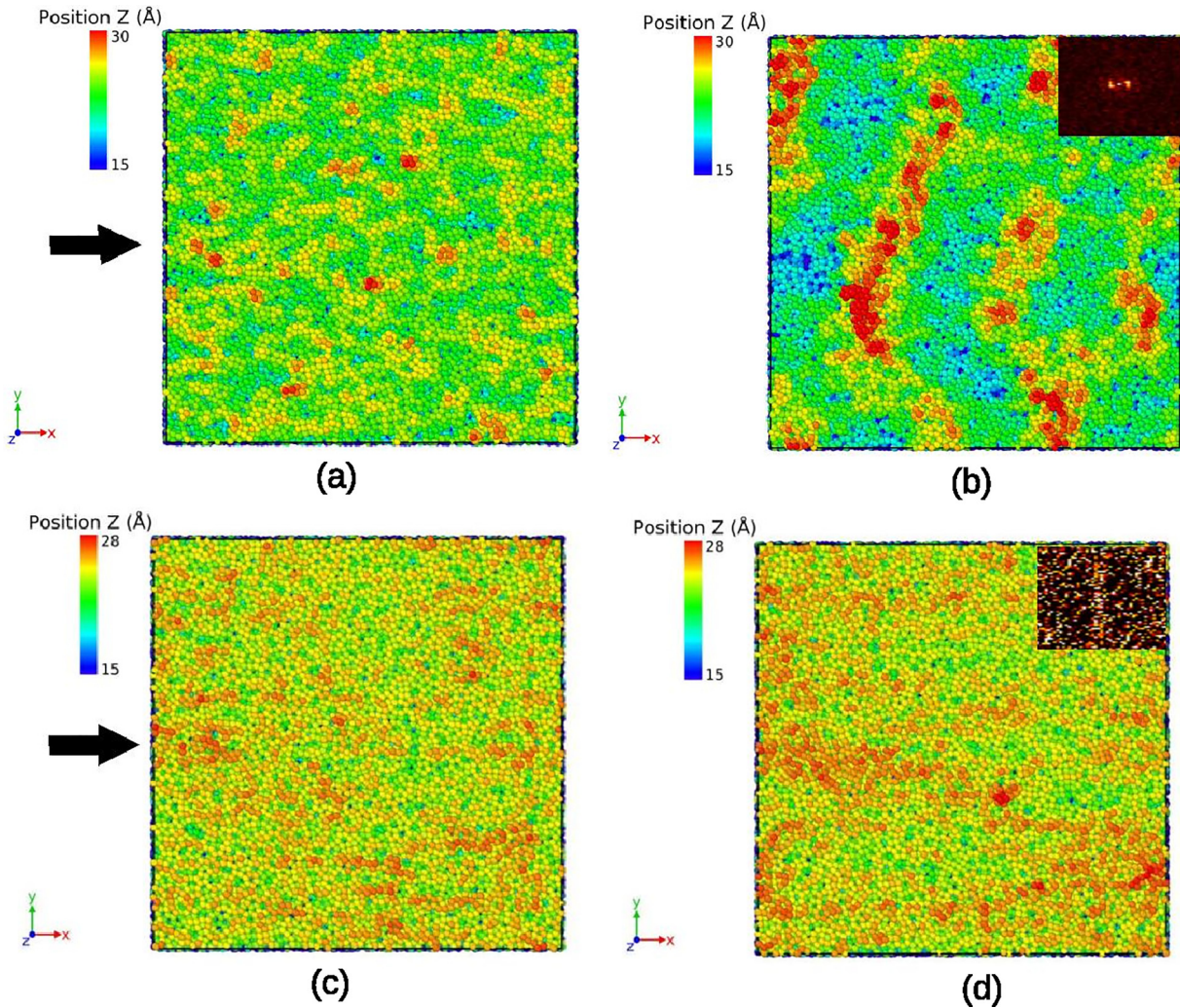


FIG. 3. Evolution of the a-Si surface under 30eV-Ar⁺ at 70° (a) 4500 and (b) 54000 impacts (adapted from result covered in Ref. [19] and including FFT of the surface); and at 85° (c) 78 000 and (d) 160 200 impacts (including FFT of the surface). The black arrow indicates the irradiation direction.

addition to this, the FFT image provided in Fig. 3(d) is also showing certain perpendicular orientation, as the one shown in Fig. 1(i), where an intense set of dots arranged perpendicular to incoming fluence can be noticed. In other words, the orientation of this line of dots is perpendicular to the one shown in Fig. 3(b).

B. Erosive and redistributive components of surface self-organization

We further analyze quantitatively the effect of erosive and redistributive components to the ripple formation process in our simulations. For completeness of the comparative analysis, we also include the case of ripple formation under the 70° incidence from Ref. [19].

Figure 4(a) shows the evolution of the cumulative number of sputtered atoms with fluence for all the simulated cases, including the 70° incidence. As expected, we see the highest sputtering dynamics under the ion beam tilted at 70° with respect to the surface normal. This value grows linearly with the number of incident ions, which is the same as for the 45° tilt. A slight increase of the growth rate is noted when the number of

incident ions is larger than 40 000 [a thin dashed line guides the eye in Fig. 4(a)], when the surface develops significant roughening. Surprisingly, no such change is observed for the ions impacting on the surface at 45°, although the roughening also appears at approximately the same fluence as clearly seen in Figs. 2(c)–2(d). The sputtering, and hence the erosive component of a surface self-organization in other two cases, is negligibly small (\sim a few tens of atoms after 160 000 Ar⁺ impacts). Overall, the effect of sputtering appears negligible under the current irradiation condition (the highest sputtering yield per incoming ion is \sim 0.03). Hence, in the following we focus mainly on the effect of atomic displacements.

We analyze the total displacement calculated according to Eq. (1) along the z and x axes in the inset of Figs. 4(a) and 4(b), respectively. The y component of the total displacement is not included, since there is no dynamics in this direction and the value fluctuates around zero. The dynamics of evolution of δ_z with the fluence in all cases show rapid initial growth with the clear tendency towards saturation. The highest value of δ_z we observe for the normal incidence, where the saturation is also reached at much higher fluences than for any other incident angles. Strictly speaking, in our simulations we have not yet

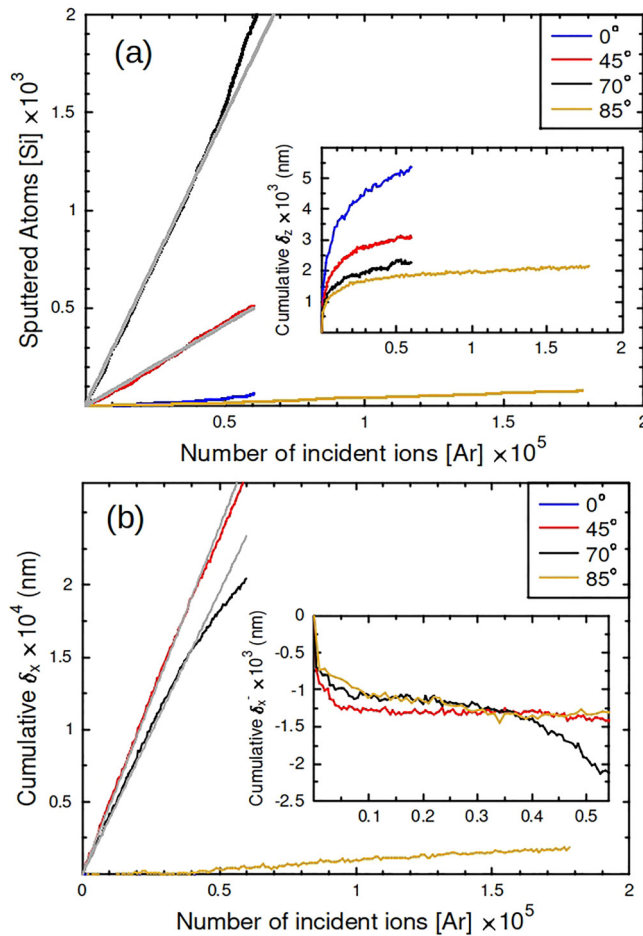


FIG. 4. (a) Evolution of cumulative number of sputtered atoms and total displacement in the z direction δ_z (in the inset) with number of ion impacts for the incident angles of 0° , 45° , 70° and 85° . (b) Evolution of total displacement in the x direction, δ_x , with number of ion impacts for the same incident angles. Inset shows the evolution of the negative component δ_x^- up to 54 000 impacts. The higher number of impacts for the grazing incidence of 85° resulted in monotonous growth of this value with the same slope. Grey dashed lines guide the eye to show the deviation from a linear growth of the number of sputtered atoms and cumulative δ_x at 45° and 70° irradiation.

reached the saturation plateau, only significant slowing of the growth rate. The saturation for 45° and 70° incident angles is more apparent, although some growth of these value may still be expected in these cases as well. For the grazing incidence of 85° , the growth still continues, even after a very high fluence. Under this irradiation condition, the displacements are rare and involve mainly individual atoms only. We note that the evolution of this component, although fairly distinct, does not show any correlation with surface self-organization, since all four plots have very similar behavior apart from the growth rate which is rising with increase of the z component of the incident momentum. However, we can clearly correlate the dynamics of the growth of this parameter with increased roughness of the surface. This process is also important as it indicates the atomic flow above the initial surface level that later on can be displaced along the surface, if a driving force for this process is provided.

More interesting behavior of the total displacement in the system is seen in the evolution of δ_x component, which is shown in Fig. 4(b). Here, we see similarly fast growth of δ_x with the fluence for both 45° and 70° incident angles, although it is clear that the growth of δ_x slows down for the 70° incidence, while it continues linearly increasing with the same initial rate for the ions impacting at 45° incidence (consistent with the single-impact results shown in Ref. [14]). We draw the thin dashed lines to guide the eye along the linear increase of δ_x for both 45° and 70° cases. For the 70° incidence, we observe a clear deviation from the linear behavior, which is explained by the accumulation of the negative displacement δ_x^- in backward direction, as it was discussed in Ref. [19], see the black line in the inset of Fig. 5(b). Here we note that similar deviation is also observed in case of the 45° incidence, but the nonlinearity in this case is much less pronounced and the ripple pattern does not emerge on the surface [see the red line in the inset of Figs. 5(b) and 2(d)].

Accumulation of δ_x under grazing incidence still shows some tendency of forward movement, however, the increase is insignificant. This result shows preferential transfer of momentum in the direction of the ion beam, although this bias is very small. δ_x for the normal incidence irradiation is omitted, since it was expected to fluctuate around zero.

We note that the high value of δ_x found for the 45° incidence does not convert directly to ripple formation [see Figs. 2(c) and 2(d)]. The single ion-irradiation model in Ref. [14], on the other hand, predicts $\theta_c = 45^\circ$ as a critical angle for ripple formation, while experimentally it is determined to be $\theta_c = 55^\circ$. Our simulations are in line with experimental observations, since we clearly see that the strong total displacement δ_x under the 45° of incidence is insufficient for ripple formation, i.e., the developed roughness does not align in this case into well-organized merged structures.

Regarding the results shown in Fig. 4(b) on 85° , we notice that the contribution in x direction fluctuates around zero. We can see that neither the accumulation of δ_x nor the sputtered atoms can directly explain the formation of the ripples over the surface, and, neither, the orientation of these. We have observed that the process starts with small displacements of the atoms, piling up and, after that, these structures merge and build the ripples. The displacements in general are short over the surface ($x - y$ plane). However, the small displacements outward from the surface (δ_z) seem to explain the formation of ridges [note that δ_z is constantly increasing in Fig. 4(a) inset]. Due to the grazing incidence, the incoming ions induce shallow effects in the surface, but the high fluence enable to create these small structures aligned to the parallel direction (perpendicular mode). The height of these structures is low, as was observed experimentally [14].

C. Displacements of surface atoms under high fluence irradiation

Since in the previous section we saw that atomic displacements play more significant role in surface self-organization under the low energy ion irradiation, at least, in the following we focus on the analysis of the displacements of the surface atoms only. By surface atoms we understand the atoms which are found within the same layer as defined in Ref. [19], i.e., the

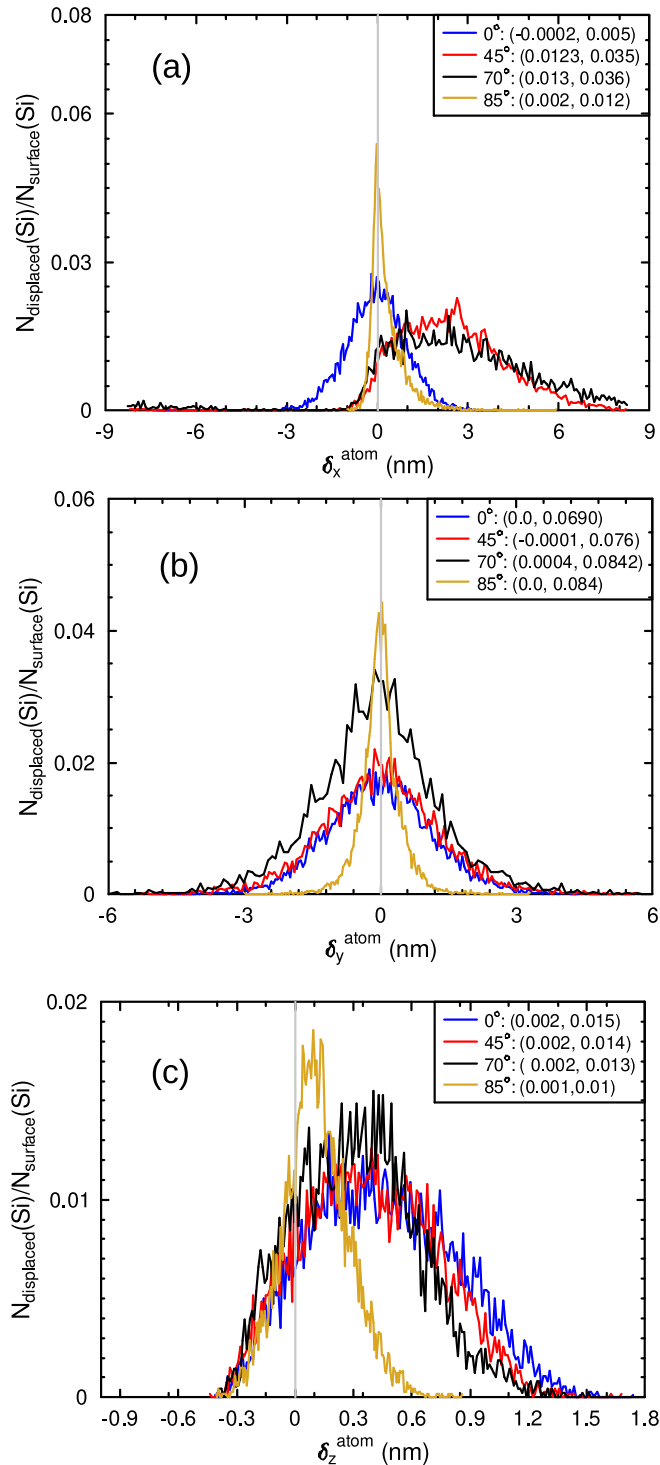


FIG. 5. Histograms of the ratio of displaced atoms [$N_{\text{displaced}}(\text{Si})$] over the total number of atoms considered in the uppermost 22 Å of the cell ($N_{\text{surface}}(\text{Si})$), sorted according to the atomic displacements ($\delta_i^{\text{atom}} = i_{\text{final}}^{\text{atom}} - i_{\text{initial}}^{\text{atom}}$) in (a) $i = x$, (b) $i = y$, and (c) $i = z$ directions at the end of the simulations. The gray thin line marks the zero displacement. The mean and standard deviation (μ, σ) of the distributions are shown in the legends.

atoms with z coordinate greater than 22 Å. This layer includes all atoms that were actively displaced due to ion impacts at the surface, contributing to the mounds of the surface roughness.

Figures 5(a)–5(c) show the histograms of the individual atomic displacements δ_i^{atom} (i stands for x , y or z) in the corresponding directions for the surface atoms that are found in the final configurations of the simulations with respect to the initial positions.

We see that the distributions of δ_x^{atom} [Fig. 5(a)] for the inclined incidence with the 45° and 70° tilts are very similar with slightly greater number of atoms displaced to larger distances for the 70° incidence. The broad distributions of δ_x^{atom} reveal a stronger tendency for collective movement of atoms, for instance, when a formed random mound has been moved along the surface. The smaller the mound, the further the displaced atoms can move, explaining a slow decreasing slope for the larger displacement values. The process is observed for both the 45° and 70° incidences, however, the self-organization is stronger in the case of the 70° incidence, which explains the slight difference in behavior of both distributions for positive displacements. We see here that the δ_x^{atom} distribution for the 45° incidence is more compact with a sharp peak at about 3 nm, which indicates that the mounds indeed could have been moving under this incidence, but only to relatively short distances. The displacements greater than 5 nm are less frequent than for the 70° incidence, which allows for stronger separation between the individual ripples and, hence, clearer self-organization structure.

The normal incidence also resulted in rather broad peak centered around zero, while the peak for the 85° incident angle is very narrow [Fig. 5(a)]. The broad peak at the normal incidence is also explained by flow of atoms and piling up into mounds, but since there is no preferential momentum transfer along the surface, there is no preferential movement of these mounds and, hence, the atoms are displaced in both positive and negative x directions with equal probability. The peak of δ_x^{atom} for 85° is very sharp and also centered near zero similarly to the distribution at the normal incidence, however, we observe a clear skewness towards positive δ_x^{atom} . This indicates that the displacements in the x direction, under the grazing incidence, contributes to atomic flow forward to a much lesser extent compared to lower ion incidence tilts, since the displacements are produced mainly in single impacts and direct momentum transfer to the collided atom with only insignificant effect of atomic flow along the surface in the x direction.

The distributions of atomic displacements in the y -direction, δ_y^{atom} , shown in Fig. 5(b), are symmetric around 0 as expected, since there is no preference in the displacement of atoms in this direction. Surprisingly, while the distributions collected for the atoms displaced under normal and 45° incidence are almost identical, the number of displaced atoms sidewise at 70° incidence is noticeably greater. This is an important observation for explaining the nature of self-organization and pattern formation, since it indicates the greater momentum transfer to the surface atoms, setting in motion many atoms collectively in every ion impact. δ_y^{atom} for 85° incidence is again distributed much narrower around zero as compared to the other distributions. In the graphs of Fig. 5(c) we observe asymmetry in all distributions, which is explained by preferential relaxation of energetic atoms towards the open surface as well as formation of surface roughness via a pileup effect. However, some of the atoms

where displaced inwards into the bulk, following the momentum transfer from the incoming ion beam. Remarkably, all distributions of δ_z^{atom} for nongrazing incidence (0° and 45°) are very similar and extend to the same height. However, the distribution of δ_z^{atom} for 70° incidence is slightly different, it shows more coherent displacements of atoms to the same distance, which is explained by formation of regular structures, such as ripples. Moreover, the ions incoming at 70° to the surface normal were apparently able to displace the atoms forward in x direction, but both in positive and negative z directions. This specific way of atomic displacements provided stronger force for self-organization as the atoms under the surface were bound more strongly and, hence, involved a larger number of atoms in the collective movement. The grazing incidence resulted in the narrower distribution of δ_z^{atom} , however, the shape and the bias towards the positive directions (outwards from the surface) is the same.

IV. DISCUSSION

Results presented in Sec. III B clearly indicate that erosive component of the ion irradiation process plays an insignificant role in surface modification processes in the considered ion energy regime. However, the dynamics of atomic displacements is very interesting and a few important observations can be deduced from its analysis. First of all, the displacements in the z direction keep increasing with fluence, although this increase slows down dramatically after surface roughness has developed. Organization of random surface features (mounds) into larger formations (ridges) slows down the growth of δ_z further. We see that the strongest decrease of the growth slope amongst the tilted incidence cases is observed for the inclination of 70° . The grazing incidence resulted in even slower growth of δ_z , which is, however, explained by much slower dynamics of modification of surface morphology compared to other studied cases. Analysis of the total displacement in the y direction, δ_y , did not reveal any interesting features.

The situation changes when the total displacement δ_x is analyzed. Here we see different behavior of increase of the cumulative total displacement with fluence. Although the inclination of 70° results in the greater momentum projection on the x axis, the growth of δ_x for 70° is slower than that for 45° . We explained this counter-intuitive result by analyzing the behavior of the negative component of δ_x^- for both angles. In the inset of Fig. 4(b) we compare the evolution of δ_x^- under the 45° and 70° incident angles (the red and black curves, respectively). We see that initially, the growth of the cumulative backward displacement is equally rapid in both cases, which is explained by linear summation of all backward displacements in the nonoverlapping individual cascades. This growth slows down again in both cases, however, more efficiently for the case of 70° . This indicates the start of cascades overlaps, which is responsible for nonlinear growth in cumulative displacements, discussed earlier in Ref. [19]. Here we emphasize that the nonlinear effect in evolution of the total displacement of surface atoms under tilted ion beam increases with increase of the tilt, i.e., with increase of the momentum transfer component along the surface.

Eventually, both δ_x^- saturate at different levels, since the shorter forward displacements that surface atoms experienced

under the 45° tilt allowed for accumulation of greater δ_x^- before the saturation. After $\sim 20\,000$ ion impacts, δ_x^- starts growing again for the 70° case with the same slope as for the 45° case, but after $\sim 45\,000$ ions (twice as many), δ_x^- decreases again. This indicates the start of self-organization, in other words, the formation of ridges from the random mounds. We also see that approximately at the same fluence (45 000 ion impacts) as the one that induced the growth of δ_x^- under 45° incidence, the slope of δ_x^- changes to a much stronger one under the 70° incident angle. The change of the slope to a more rapid one coincides with the start of a clear organization of the ripples on the surface. See Supplemental Material for a more detailed process of ripples formation at 70° incidence compared to 45° and 85° [31]. The large ridges protect backward displacements at the back of the ridge, while the forward displacements before the ridge are pushing the atoms forward. The random ridges on the surface formed under the 45° incidence do not shield sufficiently the backward displacements [see inset of Fig. 4(b)] and self-organization does not occur [see Fig. 2(d)].

Analysis of the atomic displacements δ_z^{atom} reveals that the flow of atoms in the z direction, although fairly strong, does not explain self-organization of the surface into a pattern. We see that the distributions of δ_z^{atom} for the surface atoms in all studied cases are very similar, while the atomic displacements in this direction on the surface with the most organized structures are even slightly shorter than those observed on the surfaces with random mounds, see Fig. 5(c). Clearly the atomic flow in the xy plane contributed to the self-organization to much greater extent. Although the total displacement δ_y fluctuates around zero and seemingly does not evolve with fluence, the distribution of atomic displacements δ_y^{atom} clearly indicates that the flow of atoms in this direction occurred as well [see Fig. 5(b)]. Moreover, this flow is the strongest under the 70° incidence, the case which resulted in the clear ripples on the surface.

To visualize the effect of atomic flow, in Fig. 6 we show the atomic displacements as the vectors connecting the initial positions of the surface atoms and their positions in the final snapshots. The atoms shown in these figures are the surface atoms with the z coordinate above 22 \AA . The absolute value of these displacements can be estimated from the corresponding color bars. In these figures we observe fairly small random displacement of atoms in the xy plane under the normal incidence, see Fig. 6(a), with the more significant flow in the z direction (note the color scale, but the small length of the vector projections on the xy plane.) A more intriguing situation can be seen from the comparison of Figs. 6(b) and 6(c). Here the displacement vectors for the 45° and 70° incident angles are shown, respectively. Although the absolute values of these displacements are fairly close (displacements appear mainly in green color on the same color scale), we see that there are more vectors of yellow and red colors on the surface with the 70° of the incidence, indicating stronger displacements of the surface atoms, i.e., ion-beam driven atomic flow of surface atoms. Clearly, higher mobility of surface atoms under the 70° incidence contributed to self-organization of the ripples, while the same ripples under the 45° of incidence are almost indistinguishable.

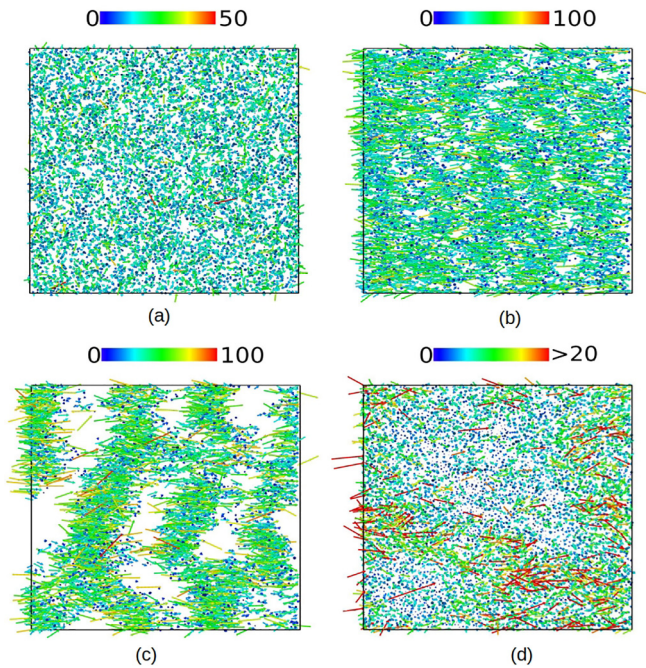


FIG. 6. Displacements evolution of the uppermost 22 Å of the cell from initial to final configuration for (a) 0° (54 000 Ar⁺) ($\alpha = 45.4320025 \pm 0.434508$), (b) 45° (54 000 Ar⁺) ($\alpha = 22.3 \pm 0.2$), (c) 70° [19] (54000 Ar⁺) ($\alpha = 21.3 \pm 0.3$) and (d) 85° (160200 Ar⁺) ($\alpha = 36.2 \pm 0.4$), colored according to their lengths in Å. The vectors are scaled 1/5 in (a)–(c) and 1/2.5 in (d) for visibility purposes.

The distribution of atomic displacements under the 85° incidence also reveal a correlation between the position of the ridges formed parallel to the ion beam, and the concentration of the longer displacements than those of the atoms that remained in the trenches between the ridges [see Fig. 6(d)]. Certainly, these atoms experienced very little displacements, while the atoms which ended up in the ridges traveled much longer distances mainly ahead but also strongly to the side. It has been suggested [32] that the transition of ripple mode from parallel to perpendicular under the grazing incidence occurs because of dominating role of erosion over mass redistribution in the ripple formation process. This conclusion was based on analysis of low-to-medium range of irradiation energies (down to hundreds of eV), known to cause fairly strong sputtering of surface atoms under grazing incidence. In the present case, under the ultralow irradiation energies, this argument does not hold as the sputtering yield is extremely low and surface erosion is very inefficient to explain surface patterning, which was observed also in experiment [33]. In our simulations, where the irradiation energy is close to the threshold displacement energy [19], we clearly see that the self-organization is still mainly driven by redistribution of surface atoms that becomes stronger the longer the grazing incidence irradiation is applied. See Fig. 6(d) and Supplementary Material (85DEGREES-SURF-FORMATION-DISP.MP4 and 85DEGREES-SURF-FORMATION-POSZ.MP4) for the effect of redistribution at grazing incidence [31].

Furthermore, we estimated the deviation of the displacement direction from the ion beam direction, i.e., from the x direction by comparing the x and y components of the

displacements [$\alpha = \tan^{-1}(\frac{\delta_{y,atom}}{\delta_{x,atom}})$]. These values are given in the parentheses in the caption of Fig. 6. Surprisingly, we see a preferential deviation of the displacements with respect to the ion beam direction, which is similar for all atoms (the obtained error bar is given by the standard error of the mean). This shows that the component perpendicular to the direction of the beam plays an important role in the self-organization process. In both cases of 45° and 70° this deviation was about 22°, which indicates preferential atomic movement in the x direction, while for 0° and 85° these deviations are 45° and 36°, respectively. The former value shows no preference in the displacements in x and y directions, while the latter shows the stronger bias of displacements in the y direction in self-organization process than that for the less tilted incidences.

To clarify further the effect of atomic displacements, we performed the BCA calculations of the cascades for several incident angles. We used the CASWIN code [34], which allows to trace the atomic trajectories observing statistical evolution of cascades. Since BCA is not reliable for energies below 1 keV [16], we have simulated the trajectories for 1 keV Ar ions in Si for all energetic atoms that received momenta in collision cascades within the very top surface layer of 5 Å. We can relate these results to the case studied by MD at much lower incident energy, since in BCA we only plot the shape of the initial cascades within the surface layer, ignoring the surface sputtering, that is irrelevant at the energies of the interest of the present work. More specifically, the BCA calculations allow us to observe the shape of momentum transfer distribution which is expected to be similar within the range of ion energies causing collision cascades. Figure 7(a) summarizes these calculations showing the color-coded trajectories, where the color indicates the energy of the atom which it had at the given point of the trajectory.

In these figures we can clearly see the size increase of the high energy spot on the two-dimensional map (see violet color in the middle of the cascades) with increase of the ion beam tilt. At the grazing incidence the spot decreases again and shrinks also laterally. The shape of the cascades under 85° is the most elongated in the x direction amongst all the presented cases. Moreover, we see that with increase of incidence the lateral spread of the cascade (y direction) becomes broader [see also Fig. 5(b)], which can explain the more efficient self-organization as the atoms receive momentum not only along the x axis, but also sideways, with significant y component. This observation is well in line with our MD results, where we see that both 45° and 70° incidences induce sufficient migration of atoms on surface, although the momentum transferred to surface atoms under the 45° of incidence is not sufficiently strong to displace atoms to large distances. The shape of the cascades at 85° is small and narrow indicating that the cascades under this incidence are shallow. In these, the side-wise spread becomes dominant although the momentum transfer in x direction exists. This explains the formation of the perpendicular mode of the ripples.

In Fig. 7(b) we illustrate schematically the change of the cascade shape within the surface with increase of the incident angle. Here the energetic part of a cascade is illustrated as an ellipsoid with the major axis aligned with the direction of the incoming ion. Below each ellipsoid, the top views

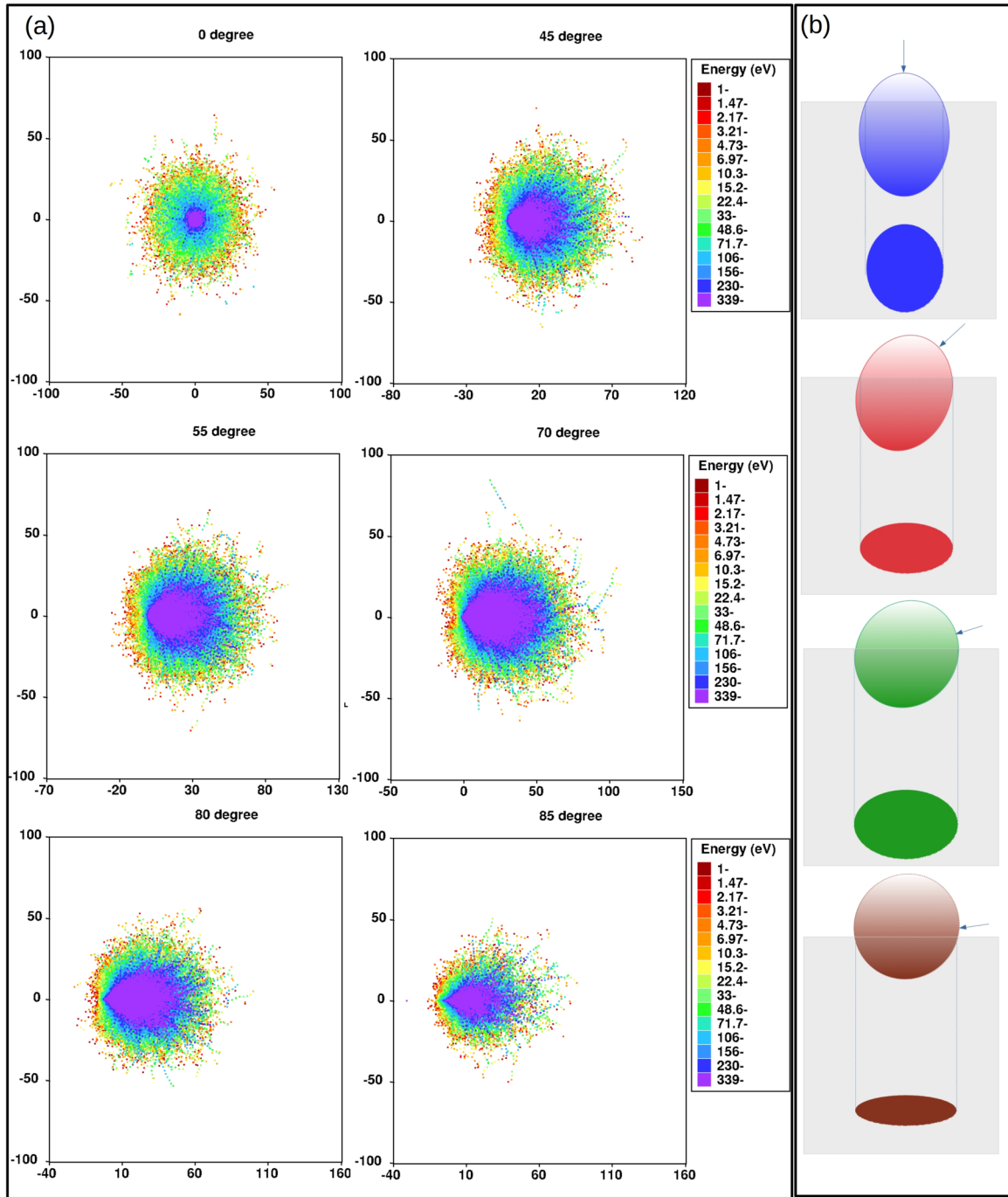


FIG. 7. (a) Maps of trajectories of atoms in BCA cascades induced by 1 keV Ar on Si for 0°, 45°, 55°, 70°, 80°, and 85°, from left to right and from top down. The trajectories are recorded only within the 5 Å surface layer and include the recoils with energies above 1 eV. The trajectories were generated from 2000 statistical ion impacts. (b) Illustration of intersections of collision cascade regions, presented in the shape of an ellipse, with the surface for a given energy of incoming ions under 0°, 45°, 70°, and 85° of incidence. The darker tone of the corresponding color represents the actual cascade inside the material (grey squares) and the lighter tone represents the missing part of the cascade. The ellipses below are the top views of the cross-sectional areas of these intersections.

on the cross-sectional areas of cascades at their intersection with the surface are shown. We see that the shape of these areas can be correlated with the momentum transfer along the surface both in the x and y directions. Clearly the surface cross section of the collision cascade at 70° has the largest

area, hence the momentum transfer along the surface in both x and y directions is the strongest. The shallow cascade under the 85° incidence results in the most narrow cross section at the surface explaining the tendency of digging the trenches parallel to the ion beam.

V. CONCLUSIONS

In conclusion, using molecular dynamics simulations we showed that the direct formation of ripples on the surface of amorphous silicon occurs only when the incident angle is greater than a threshold. We show rotation of ripple orientation with respect to the ion beam direction under the grazing incidence. We explain the dynamics of modification of surface morphology by analyzing the displacements of atoms in terms of total displacements and distributions of individual atom displacements. We clearly observe that roughness of the surface builds up as a result of atomic flow in collision cascades, however, for self-organization of the random surface features, significant atomic flow driven by tilted ion beams along the irradiated solid surface is needed. Moreover, the forward flow is complemented by the sidewise flow which is important for formation of ridges aligned at a 90° angle to the ion beam direction. At grazing incidence the sidewise flow

becomes stronger, but involves less atoms, while majority of atoms receive the momentum inwards that causes the effective “digging-in” effect forming trenches, while ridges aligned in the beam direction are formed by atoms displaced stronger on the surface. All processes require high fluences that result in displacement of large amount of atoms.

ACKNOWLEDGMENTS

The work was performed within the Finnish Centre of Excellence in Computational Molecular Science (CMS), financed by The Academy of Finland and University of Helsinki. Computational resources provided by CSC, the Finnish IT Center for Science as well as the Finnish Grid and Cloud Infrastructure (persistent identifier urn:nbn:fi:research-infras-2016072533) are gratefully acknowledged.

-
- [1] A. Fourriere, P. Claudin, and B. Andreotti, Bedforms in a turbulent stream: Formation of ripples by primary linear instability and of dunes by nonlinear pattern coarsening, *J. Fluid Mech.* **649**, 287 (2010).
- [2] R. A. Bagnold, *The Physics of Wind-Blown Sand and Desert Dunes* (Methuen, New York, 1941).
- [3] R. L. Cunningham, P. Haymann, C. Lecomte, W. J. Moore, and J. J. Trillat, Etching of surfaces with 8-keV argon ions, *J. Appl. Phys.* **31**, 839 (1960).
- [4] R. M. Bradley and J. M. Harper, Theory of ripple topography induced by ion bombardment, *J. Vac. Sci. Technol.* **6**, 2390 (1988).
- [5] G. Carter and V. Vishnyakov, *Phys. Rev. B* **54**, 17647 (1996).
- [6] S. A. Norris, J. Samela, C. S. Madi, M. P. Brenner, L. Bukonte, M. Backman, F. Djurabekova, K. Nordlund, and M. J. Aziz, MD-predicted phase diagrams for pattern formation, *Nat. Commun.* **2**, 276 (2011).
- [7] S. A. Norris, Stability analysis of a viscoelastic model for ion-irradiated silicon, *Phys. Rev. B* **85**, 155325 (2012).
- [8] S. A. Norris, Stress-induced patterns in ion-irradiated silicon: Model based on anisotropic plastic flow, *Phys. Rev. B* **86**, 235405 (2012).
- [9] A. Moreno-Barrado, M. Castro, R. Gago, L. Vazquez, J. Munoz-García, A. Redondo-Cubero, B. Galiana, C. Ballesteros, and R. Cuerno, Nonuniversality due to inhomogeneous stress in semiconductor surface nanopatterning by low-energy ion-beam irradiation, *Phys. Rev. B* **91**, 155303 (2015).
- [10] J. Muñoz-García, R. Cuerno, and M. Castro, Stress-driven nonlinear dynamics of ion-induced surface nanopatterns, *Phys. Rev. B* **100**, 205421 (2019).
- [11] S. Facsko, T. Dekorsy, C. Koerdter, C. Trappe, H. Kurz, A. Vogt, and H. L. Hartnagel, Formation of ordered nanoscale semiconductor dots by ion sputtering, *Science* **285**, 1551 (1999).
- [12] D. Chowdhury, D. Ghose, and B. Satpati, Production of ordered and pure Si nanodots at grazing ion beam sputtering under concurrent substrate rotation, *Mater. Sci. Eng. B* **179**, 1 (2014).
- [13] H. Hofsäuss, K. Zhang, H. G. Gehrke, and C. Brüsewitz, Propagation of ripple patterns on Si during ion bombardment, *Phys. Rev. B* **88**, 075426 (2013).
- [14] A. Lopez-Cazalilla, D. Chowdhury, A. Ilinov, S. Mondal, P. Barman, S. R. Bhattacharyya, D. Ghose, F. Djurabekova, K. Nordlund, and S. Norris, Pattern formation on ion-irradiated Si surface at energies where sputtering is negligible, *J. Appl. Phys.* **123**, 235108 (2018).
- [15] S. A. Norris, M. P. Brenner, and M. J. Aziz, From crater functions to partial differential equations: A new approach to ion bombardment induced nonequilibrium pattern formation, *J. Phys.: Condens. Matter* **21**, 224017 (2009).
- [16] A. Lopez-Cazalilla, A. Ilinov, L. Bukonte, F. Djurabekova, K. Nordlund, S. Norris, and J. Perkinson, Simulation of atomic redistribution effects in a-Si under ion irradiation, *Nucl. Instrum. Methods Phys. Res. B* **414**, 133 (2018).
- [17] A. Lopez-Cazalilla, A. Ilinov, F. Djurabekova, and K. Nordlund, Modeling of high-fluence irradiation of amorphous Si and crystalline Al by linearly focused Ar ions, *J. Phys.: Condens. Matter* **31**, 075302 (2019).
- [18] C. Fridlund, J. Laakso, K. Nordlund, and F. Djurabekova, Atomistic simulation of ion irradiation of semiconductor heterostructure, *Nucl. Instrum. Methods Phys. Res. B* **409**, 14 (2017).
- [19] A. Lopez-Cazalilla, F. Djurabekova, A. Ilinov, C. Fridlund, and K. Nordlund, Direct observation of ion-induced self-organization and ripple propagation processes in atomistic simulations, *Mater. Res. Lett.* **8**, 110 (2020).
- [20] Z. Zhou, J. Cui, Q. Hou, and K. Zhang, Role of mass redistribution on nanoripple formation and propagation: A molecular dynamics simulation study, *Appl. Surf. Sci.* **585**, 152630 (2022).
- [21] C. S. Madi and M. J. Aziz, Multiple scattering causes the low energy–low angle constant wavelength topographical instability of argon ion bombarded silicon surfaces, *Appl. Surf. Sci.* **258**, 4112 (2012).

- [22] M. Ghaly, K. Nordlund, and R. S. Averback, Molecular dynamics investigations of surface damage produced by keV self-bombardment of solids, *Philos. Mag. A* **79**, 795 (1999).
- [23] K. Nordlund, M. Ghaly, and R. S. Averback, Mechanisms of ion beam mixing in metals and semiconductors, *J. Appl. Phys.* **83**, 1238 (1998).
- [24] M. Z. Bazant, E. Kaxiras, and J. F. Justo, Environment dependent interatomic potential for bulk silicon, *Phys. Rev. B* **56**, 8542 (1997).
- [25] J. F. Justo, M. Z. Bazant, E. Kaxiras, V. V. Bulatov, and S. Yip, Interatomic potential for silicon defects and disordered phases, *Phys. Rev. B* **58**, 2539 (1998).
- [26] K. Nordlund, N. Runeberg, and D. Sundholm, Repulsive interatomic potentials calculated using hartree-fock and density-functional theory methods, *Nucl. Instrum. Methods Phys. Res. B* **132**, 45 (1997).
- [27] C. Kittel, *Introduction to Solid State Physics*, 3rd ed. (Wiley, New York, 1968).
- [28] O. Lozano, Q. Y. Chen, B. P. Tilakaratne, H. W. Seo, X. M. Wang, P. V. Wadekar, P. V. Chinta, L. W. Tu, N. J. Ho, D. Wijesundera, and W. K. Chu, Evolution of nanoripples on silicon by gas cluster-ion irradiation, *AIP Adv.* **3**, 062107 (2013).
- [29] H. J. C. Berendsen, J. P. M. Postma, W. F. van Gunsteren, A. DiNola, and J. R. Haak, Molecular dynamics with coupling to external bath, *J. Chem. Phys.* **81**, 3684 (1984).
- [30] The MathWorks Inc., Statistics and machine learning toolbox documentation, Natick, Massachusetts (2022), <https://www.mathworks.com/help/stats/index.html>.
- [31] See Supplemental Material at <http://link.aps.org/supplemental/10.1103/PhysRevMaterials.7.036002> for additional information on the full evolution of the simulations, mean displacement and analysis of the mounds formed at different irradiation angles..
- [32] H. Hofsäss, Surface instability and pattern formation by ion-induced erosion and mass redistribution, *Appl. Phys. A* **114**, 401 (2014).
- [33] D. Chowdhury and D. Ghose, *Adv. Sci. Lett.* **22**, 105 (2016).
- [34] L. Bukonte, F. Djurabekova, J. Samela, K. Nordlund, S. A. Norris, and M. J. Aziz, Comparison of molecular dynamics and binary collision approximation simulations for atom displacement analysis, *Nucl. Instr. Meth. Phys. Res. B* **297**, 23 (2013).